Topical Review for Semiconductor Science and Technology

Review of Amorphous Silicon Based Particle Detectors: The Quest for Single Particle Detection

N. Wyrsch, C. Ballif.
Ecole Polytechnique Fédérale de Lausanne (EPFL), Institute of Microengineering (IMT), Photovoltaics and thin-film electronics laboratory, Breguet 2, 2000 Neuchâtel, Switzerland,

Abstract. Hydrogenated amorphous silicon (a-Si:H) is attractive for radiation detectors because of its radiation resistance and processability over large areas and with mature Si microfabrication techniques. While the use of a-Si:H for medical imaging has been very successful, the development of detectors for particle tracking and minimum-ionizing-particle detection has lagged, with almost no practical implementation. This paper reviews the development of various types of a-Si:H-based detectors and discusses their respective achievements and limitations. It also presents more recent developments of detectors that could potentially achieve single particle detection and be integrated in a monolithic fashion into a variety of applications.

Keywords: amorphous silicon, particle detectors, radiation hardness, monolithic device

1. Background

1.1 Motivations

Among possible materials for detectors, hydrogenated amorphous silicon (a-Si:H) is one of the most radiation-resistant semiconductors and is therefore very attractive for the fabrication of particle sensors [1]. The fact that this material can be deposited on various types of substrates and alloyed with other elements to modify its properties is another crucial advantage. a-Si:H has been successfully implemented in large-area particle detectors for X-ray radiography using an indirect detection scheme. However, despite more than 30 years of research, this technology has hardly been used as particle detectors in experiments or systems that rely on direct detection. One of the reasons is the failure to demonstrate detection of single, high-energy particles.

In this topical review we present the development of a-Si:H-based particle detectors and in particular (but not only) strategies aiming at minimum ionizing particles (MIPs) and single particle detection. To this purpose, we discuss in detail the detection capability and the fundamental limits and bottlenecks (and the possible solution to overcome them) of this thin-film technology. In this context, some recent developments are presented in more detail. They comprise the possibilities of vertical integration of a thick a-Si:H diode array on top of a readout ASIC (the so-called "thin-film on ASIC" or "TFA" technology) as well as vertically integrated microchannel plates (MCP). The possibility of depositing a-Si:H over a large area, on various substrates, and micro-machining the layers is also opening various opportunities in the field of particle detectors. The high radiation hardness of a-Si:H together with the ability to process this material offers the potential for implementation in experiments in colliders with high luminosity, e.g. future LHC (Large Hadron Collider) upgrades [2].

1.2 a-Si:H material and technology

The first investigation of a-Si:H was reported by Chittik et al. in 1969 [3]. It was observed that the growth of this material from plasma-enhanced chemical vapour deposition (PE-CVD, also referred to as glow discharge) from silane (SiH_4) led to a much lower defect density compared to evaporated or sputtered amorphous silicon. The development of a-Si:H technology in the 70's [4] and especially the demonstration that it can be substitutionally doped (n-type and p-type) by Spear

and Lecomber in 1975 [5] spurred the development of various types of devices such as transistors [6], solar cells [7] and memories [8].

a-Si:H material is a disordered semiconductor. The irregular arrangement of atoms has the consequence that not all Si-Si bonds can be satisfied and leads to the presence of broken or dangling bonds (DBs). Hydrogen is thus introduced into the material to passivate those DBs which act as defects and recombination centres. The minimum amount of H necessary to passivate most of the DBs is about 1% atomic. The H content in the material has an influence on its bandgap (increasing the hydrogen content enlarges the bandgap) and depends on the deposition conditions such as the deposition temperature. The typical H content of the material deposited by PE-CVD is usually around 10% atomic. a-Si:H material is generally deposited at temperatures around 200°C from the dissociation of silane SiH_4. H is generally added to dilute the silane and improve the resulting material properties. Deposition temperatures as low as 100°C are possible but lead to more defective (and less dense) material while the highest possible deposition temperature is given by the start of the desorption of H at around 350°C. This relatively low processing temperature allows for the deposition of layers or devices on a variety of substrates [9] and even on top of sensitive devices such as CMOS (Complementary Metal-Oxide Semiconductor) chips, as discussed below in section 3.

Several deposition techniques are available for electronic-quality a-Si:H: PE-CVD with plasma excitation at the radio frequency used for industrial processes (RF at 13.56 MHz) [10], at very-high frequencies (VHF, between 27 and 150 MHz) [11] or at microwave frequencies [12], or alternatively hot-wire (HW) deposition (also known as catalytic CVD) [13]. All techniques cited above have been able to produce high-quality a-Si:H material and have been successfully used, at least in the laboratory, for a-Si:H device fabrication. However, each one of them offers specific advantages and disadvantages in terms of deposition area, deposition rate or material properties. Doping is achieved by adding PH_3 to the process gas (e.g. mixture of silane SiH_4 and H) for n-type material and by adding B_2H_6 or TMB (Trimethylboron) for p-type material.

The disordered nature of a-Si:H leads to under-coordinated Si atoms (atoms with one or more DBs) and the resulting DBs lead to the presence of a continuous distribution of states within the bandgap. States can be classified as extended states in the valence and conduction bands with a finite mobility, or as localized states comprising DB states in the centre of the bandgap and conduction and valence band tail states. These tail states exhibit an approximately exponential shape as a function of energy, and their width (which depends on the magnitude of the disorder) is asymmetric (larger on the side of the valence band). Strictly speaking, therefore, a-Si:H does not have a bandgap but a mobility gap, as carriers located in localized states have zero or very low mobility [14]. An optical gap is also commonly defined to characterize optical absorption, which reflects the distribution of states in the bandgap and band edges. Often reported are Tauc optical gaps [15] or E_{04} values. E_{04} is defined as the photon energy for which an optical absorption coefficient of 10000 cm^{-1} is measured. Typical bandgap values depend on the metric used and on the material properties (mainly on the H content [16]) and are around 1.7 to 1.8 eV.

a-Si:H has been so far treated as a continuous random network of atoms with isolated randomly distributed DBs as the defect sites and randomly distributed hydrogen atoms. However, this view is challenged by the observation of the predominance of hydrogenated di-vacancies in a dense a-Si:H network and the predominance of hydrogenated nano-sized voids in less dense a-Si:H [17,18]. Increasing the presence of atomic H in the plasma (supplied from the decomposition of silane or added to silane) can lead to a deposition regime with the growth of crystalline phases in the material. a-Si:H deposited at the onset of the crystalline growth is often sought for high-quality devices [19]. The lowest defect density is usually obtained at low deposition rates [20]. Transitional material of high quality that incorporates nano-crystals embedded in an amorphous Si tissue, so-called polymorphous material [21], is also getting attention for use in devices.

Given its relatively wide bandgap and its disordered nature leading to a low charge carrier mobility, a-Si:H is a semi-isolating material with resistivity values higher than 10^{10} Ωcm^{-1}. This resistivity can be varied by more than 7 orders of magnitude by p- or n- doping [5]. As transport take place in extended states, conductivity is thermally activated. DBs play an important role as the main recombination centres. Doping of the material also creates additional defects (additional DBs) through a chemical equilibrium process, which rapidly degrades the quality and, as a

consequence, the carrier lifetime of the material [22]. Doped layers therefore cannot be used as active layers in photodiodes or particle sensors.

a-Si:H exhibits metastable material properties. Upon light soaking, photoconductivity and dark conductivity decrease with time and saturate after several hours or days. Annealing of the material for several hours at temperatures ≥150°C reverses the change [23]. This effect, known as the Staebler-Wronski effect (SWE), is due to an increase in the density of DBs created by the breaking of Si-Si weak bonds. The creation of additional DBs is not directly linked to photon absorption but to recombination events. A similar defect creation mechanism can therefore be observed when electron-hole (e-h) pairs recombine following double injection (in the absence of illumination) [24]. Several models have been proposed to give a microscopic description of the SWE but so far with no satisfactory result [24]. It is, however, established that the SWE is related to the H content and H bonding [25]. More detailed information on the metastability of a-Si:H and how it influences the material or device properties can be found in reference textbooks [26,27].

As discussed in the following sections, the design of a-Si:H particle detectors may require the deposition of rather thick layers. Deposition of dense a-Si:H usually results in the presence of compressive mechanical stress in the material. This stress often depends on the H content in the film [28,29] and as a consequence on the deposition conditions [29,30]. In addition, a thermal expansion coefficient mismatch between the substrate and a-Si:H may play a significant role (increasing or reducing the mechanical stress). The deposition temperature, which has a strong influence on both the H content and the resulting stress due to thermal expansion mismatch, is a key parameter for stress management to avoid any delamination of the films [31].

1.3 a-Si:H for particle detection (detection scheme and requirements)

Particle detection using an a-Si:H-based device is usually achieved either directly using thick diodes or indirectly using a thin photodiode coupled with a scintillator. In case of direct detection, the e-h pairs generated by ionization (interaction of the particles within the a-Si:H absorber) are collected on the diode. A thick diode is necessary as interactions of ionizing particles with the a-Si:H generate a small number of e-h pairs per unit length. For energetic charged particles, the energy loss per unit distance is roughly proportional (Bethe-Bloch formula [32]) to the atomic number and to the density of the material. Given the stopping power (most probable) value at minimum ionization of 1.66 MeV cm^2g^{-1} for a MIP in c-Si one can expect the creation of about 108 e-h pairs per micron of material crossed. Experimentally, a value of 80 e-h pairs is observed (related to the average value of the energy loss). The values for a-Si:H are similar but not known with confidence as complete charge collection is usually not achieved. Furthermore, as discussed in section 2.1, a large scattering is observed in experimental values of the energy needed to create e-h pairs.

In case of high energy photons, the energy loss also highly depends on the particle energy and the interacting material. The interaction by photoemission or Compton effect results in the production of an energetic electron that leads to e-h pair generation. As a consequence higher Z materials exhibit larger photon attenuation coefficients and thick detectors are needed for Si. At higher photon energy interaction occurs by direct e-h pair production and the attenuation coefficient of photon with a Si detector is well below 0.1 cm^{-1}, meaning that any Si detector is almost transparent to such X-ray. Only a fraction of the photon energy can thus be collected and as thick as possible detectors are required. For indirect detection, a scintillating material is used to convert the ionizing radiation into visible or UV photons by luminescence. In this case, a much thinner photodiode can be used. A schematic drawing of the two detection schemes is given in Figure 1.

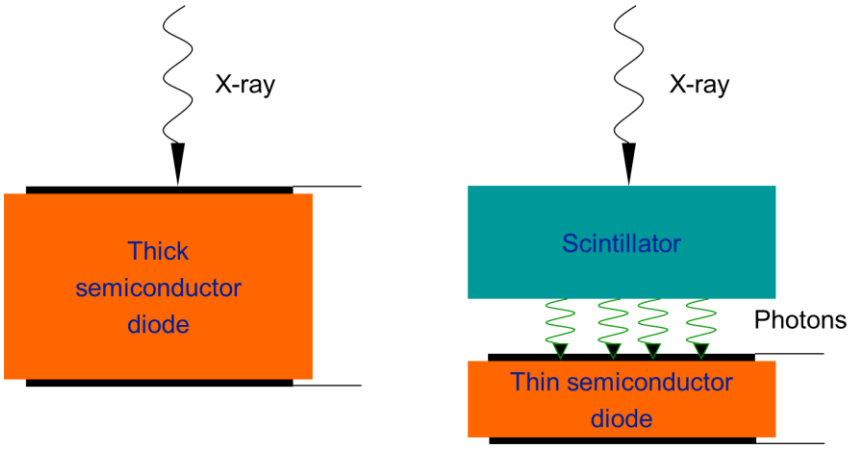

Figure 1: Schematic particle detection schemes of X-rays: Direct detection using a thick diode (left) and indirect detection using a thin diode and a scintillating layer (right).

An n-i-p (n-doped, intrinsic and p-doped layers) diode structure is used to collect e-h pairs created either by the ionizing particle (charged particles or photons), depending on the detection scheme. As indicated in the previous section, the intrinsic layer is the only active layer, and doped layers should be as thin as possible to minimize parasitic absorption. In both cases, a full depletion of the diode should be achieved as only e-h pairs generated within the depletion region can be collected and therefore can contribute to the signal. As discussed in section 2.2, this requirement is especially critical for direct detection where thick diodes are mandatory. High-quality material is required but the leakage (or dark) current, which strongly increases with bias voltage (see Figure 2), usually limits the range of useful diode thickness. At low bias voltage, the dark current is essentially given by thermal carrier emission from the bulk and depends on the material quality and intrinsic layer thickness. As the electric field increases, injection from the doped layer and the Poole-Frenkel effect in the high-field region (close to the p-i interface) become dominant.

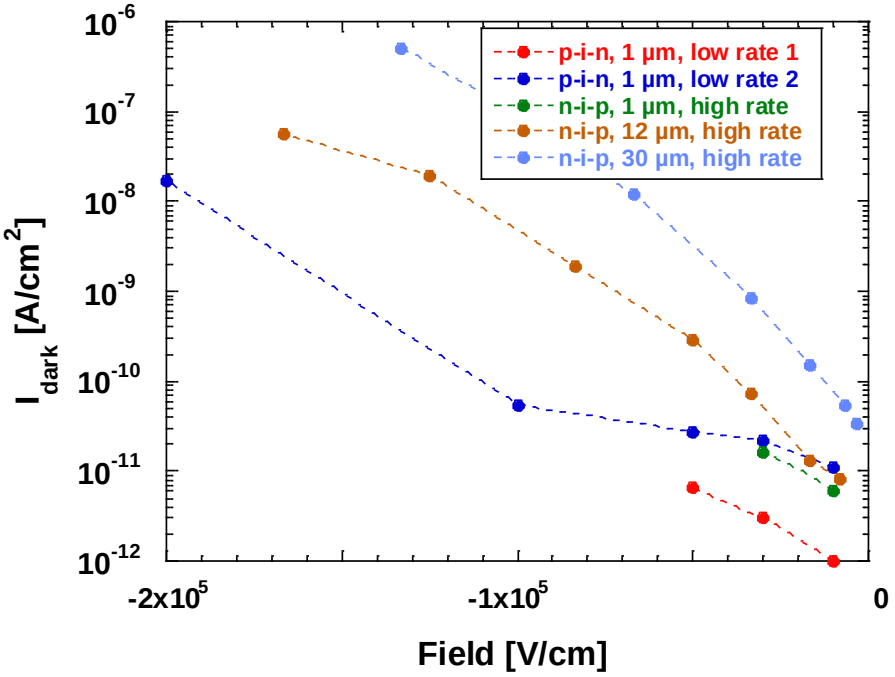

Figure 2: Leakage current of a-Si:H diodes of various thicknesses deposited at a low rate (about 0.3 nm/s and two different H dilutions of silane) and at a high rate (1.5 nm/s) (from [33]).

In order to minimize this sharp increase of leakage current with growing electric field, several solutions have been proposed in the literature: (a) An increase of the p-layer thickness [34,35], (b) the introduction of a double p-layer [36] or (c) a buried p-layer [35], or (d) the introduction of a buffer layer at the p-i interface [37].All these solutions can be easily implemented and require minimal modifications of the fabrication process. However, it is not yet clear which solution offers the lowest leakage current as interface properties (rather than the intrinsic or doped layer properties) usually play the major role in controlling leakage. Practically, the signal current given by the number of e-h pairs created and the electric field necessary to achieve full depletion should be much higher than the leakage current for this electric field value. The optimum thickness is the highest one for which this condition is satisfied. Additionally the readout electronics also has to accommodate this DC current leakage. In order for the diode to sustain a high reverse bias with low leakage, it is necessary to have a well-defined metal contact on one side of the diode and to etch the doped layer around that contact [34]. In designing the detection device, one has also to keep in mind that the defect density, and as a consequence leakage current, may increase as a function of material irradiation due to additional defect creation.

The difficulty to achieve full collection on thick a Si:H diodes (as discussed in section 2.2) and the higher signal-to-noise ratios that could be obtained from the combination of thin a-Si:H photodiode coupled with CsI scintillator led to a shift of the interest to indirect detection scheme [36]. The integration of a Si:H photodiodes in an active matrix of a Si:H based transistors here allows for spatial detection and imaging.

For indirect detection, thin devices are sufficient to absorb all the photons emitted by the scintillator. Low dark current is still necessary and low defect density material is required. However, achieving full depletion at low bias voltage is not an issue here. In case of scintillators emitting in the UV range, a critical diode design may be necessary to minimize parasitic absorption in the contact or doped layers of the diode (layers which are not photovoltaically active). A possible solution to overcome this problem is shown below in section 4.

Note also that a-Si:H layers may also be used as resistive or protective layers in other types of particle detectors. Such application usually relies on the high resistivity of a-Si:H. This material was, for example, used very successfully as spark protection layers in GridPix gaseous proportional detectors [38,39].

2. a-Si:H diode as a particle detector

2.1 Charge particle detectors

Development of charged particle (proton and alpha) detectors based on thick a-Si:H diodes was pioneered by the group of Perez-Mendez at the University of California, Berkeley [40,41] which also achieved the first detection of MIPs from various radioactive sources [42,43]. Several other groups rapidly developed similar detectors in France [44,45], in Italy [46], in Japan [47] and in Switzerland [48]. Detectors of various thicknesses from a few microns to 50 microns were investigated for the detection of various types of particles. High radiation hardness was also demonstrated, rendering a-Si:H very attractive for radiation detectors (see section 2.4). However the signal-to-noise ratio for MIPS detection using the direct detection scheme was not high enough (values between 2 and 3) [43,49] to allow for single particle detection and to allow for particle tracking.

While thick detectors are desirable to generate the maximum number of e-h pairs, the applied electric field, in many cases, could not be high enough to ensure full depletion. In this case, only the charge pairs generated in the depletion region can be collected before recombination, leading to incomplete charge collection. Signal formation is given by the drift of the e-h pairs in the intrinsic layer of the diode and therefore depends on the distance travelled. Full collection is achieved when both the electron and the hole from a generated pair are collected at the diode contacts [44]. Analysis of the signal pulse shape shows a fast contribution (due to electrons) and a much slower contribution (due to holes) given by the carriers' respective drift mobility values. In practical experiments, hole collection is difficult to record as the signal is difficult to resolve [50].

The e-h pair generation is characterized by the mean energy W needed to create one e-h pair. A linear relationship has been observed between W and the optical gap with a value of 3.6 for c-Si

(crystalline silicon) [51]. First measurements indicated a value of W=6 eV consistent with this relationship [42]. However, more detailed analysis indicated this value to be overestimated due to incomplete charge collection and found the mean W value to be between 3.4 and 4.4 eV [50]. W for a-Si:H is therefore quite close to that of c-Si. The reason why a-Si:H does not follow the usual relationship is not understood.

Energy loss in the material by a MIP is proportional to the density and atomic number. The interaction of MIPs with Si or a-Si:H results in a small number of e-h pairs generated per unit distance. In order to increase this number of e-h pairs generated in the intrinsic layer, one can use a heavier metal electrode as the diode contact (on the incoming side of the diode). Interaction of the MIP with the metal layer will create a shower of e-h pairs, leading to the injection of some of them in the intrinsic layer, leading to an increased number of collected charges [48,52]. Increase of the signal by up to a factor of 2 has been reported when replacing Al with Au contacts on state-of-the-art a-Si:H thick diodes [48].

Recently, large-area 4×1.5 cm^2 a-Si:H particle detectors deposited on glass were developed by our group to be implemented in front of the magnetic septum of a synchrotron to monitor an extraction beam. It is to our knowledge the first practical implementation of an a-Si:H detector in a high-energy physics experiment. Figure 3 shows the response of such a 5-µm-thick detector exposed to a variable fraction of a 250 MeV proton beam. A very high linearity of the signal (collected charge) as a function of the proton flux can be observed in this fully depleted a-Si:H, demonstrating both the linear response of the detector to the number of impinging protons (independently of the position) and its the spatial uniformity.

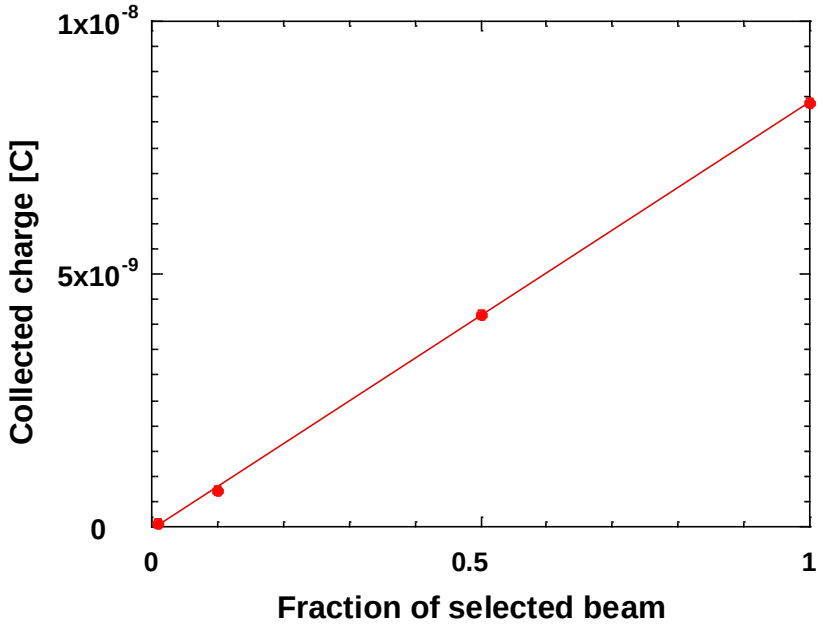

Figure 3: Charge collected (from the integral of the current during one spill) as a function of a 250 MeV proton beam fraction seen by a 6 cm^2 detector situated in the magnetic septum of a synchrotron [53].

2.2 Depletion condition and material requirements

As already stated above, only e-h pairs generated within the depletion region can be collected. Thus, to maximize the number of pairs collected, this region should extend throughout the intrinsic layer thickness. Assuming a constant density of ionized defects as a function of distance from the p-i interface, the minimal voltage V_F necessary to fully deplete a diode is given by [54]:

$$V_F = \frac{qN_{db}^{*}d^2}{2\varepsilon_0\varepsilon_{aSi}} \quad (1)$$

where N_{db}^{*} is the density of ionized dangling bonds, ε_0 is the vacuum permittivity, ε_{aSi} is the permittivity of amorphous silicon and d is the intrinsic layer thickness. In a-Si:H, the ratio of ionized defects was found to be about 30–35% [55]. A shown in Figure 4, the voltage needed for full depletion grows quadratically with thickness and reaches a value of about 1000 V (or a mean electric field of $2x10^5$ Vcm^{-1}) for a 50-µm-thick diode. Increasing the thickness while keeping full depletion results in an increase of the electric field that concentrates in the vicinity of the p-i interface and in a higher risk of breakdowns. However, such a high field will result (as seen in Figure 2) in unacceptable leakage current values. Assuming a drift electron mobility of 3 $cm^2V^{-1}s^{-1}$, a generation of 100 e-h pairs per micron and a collection of 50% the charge transit time at 1000 V is 8.3 ns, which results (if charge trapping is neglected) in a peak current of 4.8×10^{-8} A, a value much lower than the leakage current. This diode is clearly not suited for MIP detection, and the strategy to target the highest diode thickness cannot be successful. The use of moderately thick detectors is therefore advisable.

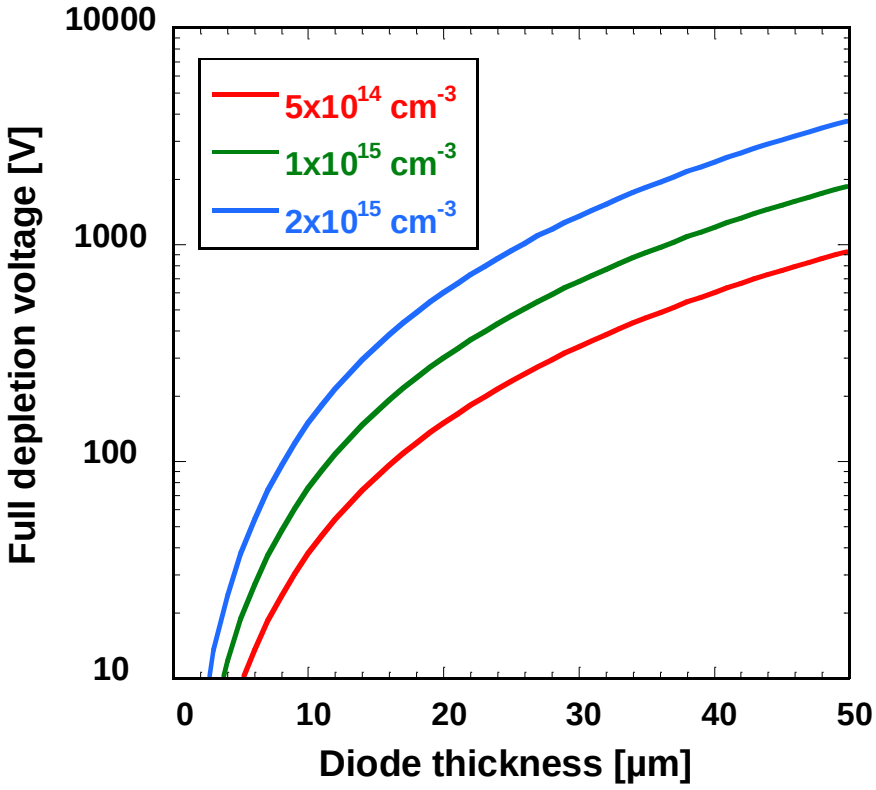

io

Figure 4: Minimum voltage necessary to fully deplete an a-Si:H n-i-p diode as a function of diode thickness and ionized defect density.

In order to reduce as much as possible the defect density and, as a consequence, the needed full depletion voltage, helium dilution of silane has been proposed. Diodes with an ionized defect density as low as 7×10^{14} cm^{-3} have been obtained [54,56]. However, similar defect densities have also been obtained with hydrogen dilution (and without He) [57]. As an alternative way to reduce the voltage needed for full depletion, Morosanu et al. proposed to slightly p-type dope the intrinsic layer. The procedure was successfully used in detectors with a thickness of up to 50 µm [58].

2.3 Other particle detection

a-Si:H detectors have also been designed for the direct detection of X-rays, gamma rays, electrons, neutrons and ions (in addition to protons and alpha particles). Detection of X-rays or gamma rays could be achieved with thick diodes as designed for MIP detection [59]. However the detection of such particles using an indirect scheme was found to more effective. Detection of neutrons requires a reactive layer. Different designs have been proposed in the literature with, for example, a combination a-Si:H diodes with Gd [60] or with ^{10}B layers [61]. One could also incorporate a ^{10}B-rich semiconductor directly into an a-Si:H-based device.

2.4 Radiation resistance of a-Si:H

The high radiation hardness of a-Si:H was recognized very early, and this property was one of the driving forces behind the development of detectors for high-energy physics experiments or for medical imaging [62]. Several irradiation tests were performed using proton [47,63,64,65], gamma [66], neutron [42], or heavy ions irradiation [67] on thin or thick p-i-n devices. For thin devices, in most cases, experiments were carried out to study the effect of irradiation on the photovoltaic properties for space applications. Figure 5 shows the effect of exposure to a displacement dose on solar cell efficiency for various semiconductors. a-Si:H is found to be one of the most radiation-resistant semiconductors.

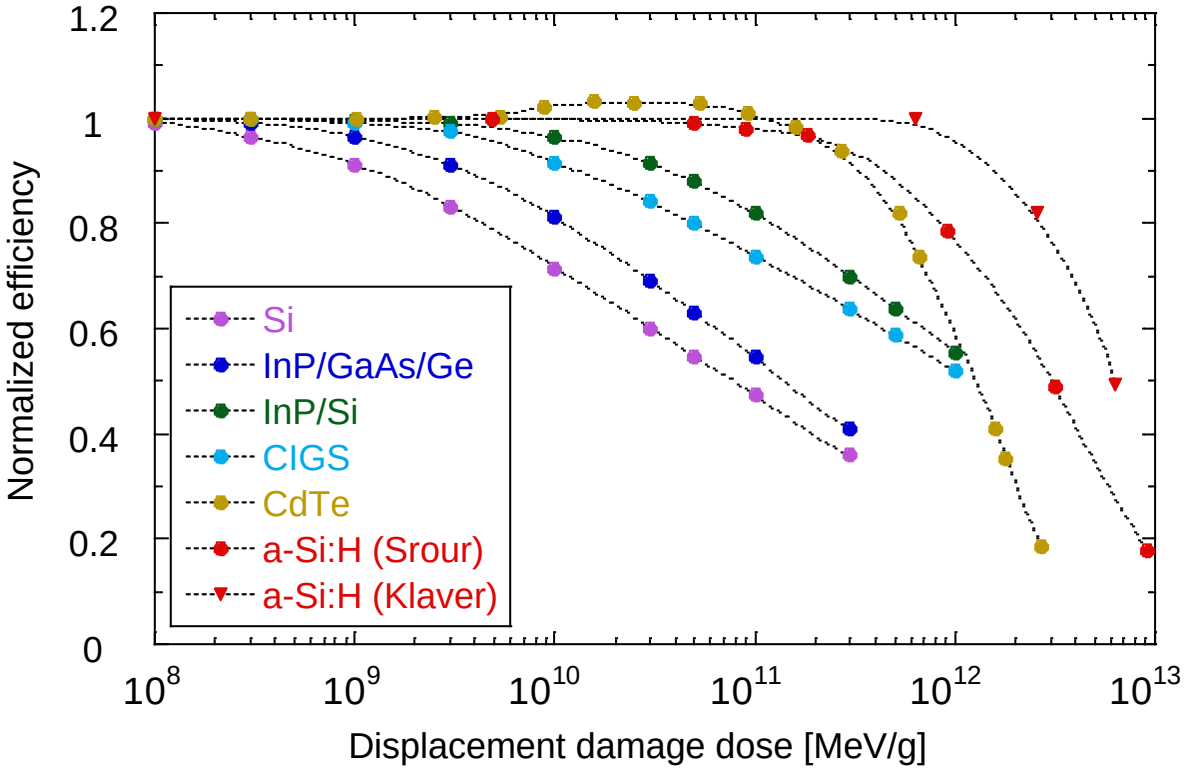

Figure 5: Effect of irradiation, expressed as displacement damage dose, on the normalized solar cell efficiency of several PV technologies (from Bätzner et al. [68], Srour [63] and Klaver [69]).

Proton irradiation tests were performed at CERN on thick a-Si:H diodes to get more insight into defect formation and metastability. 32-µm-thick a-Si:H diodes were exposed to a 24 GeV proton beam in the "IRRAD1" facility up to fluences of 2×10^{16} protons/cm^2 [70]. Figure 6 shows the current induced by the proton spills (120-ms-long periods of "beam on" with an average fluence of 1.3×10^{11} protons). One can observe a slow degradation of the detector response with fluence which tends to saturate at higher fluences ($\geq10^{15}$ protons/cm^2 [70]) at a value approximately equal to half of the initial value. An interesting self-annealing effect, related to the metastability of the material (similar to SWE), is also observed when the irradiation was stopped

for 20 hours. Within the same study, similar samples were also irradiated with lower energy protons of 405 keV. It was observed that these protons are much more effective at creating defects. These additional defects then reduce the internal field and charge collection. At these energy levels, protons – i.e. hydrogen atoms – are implanted in thick diodes and full recovery of the initial properties by annealing is no longer possible (in contrast to thinner diodes where protons are not stopped inside the device) [70]. In contrast to proton irradiation, electron irradiation creates metastable defects that can be fully annealed out [71,72]. Note that effects of electron irradiation at energies much above 1 MeV are not known.

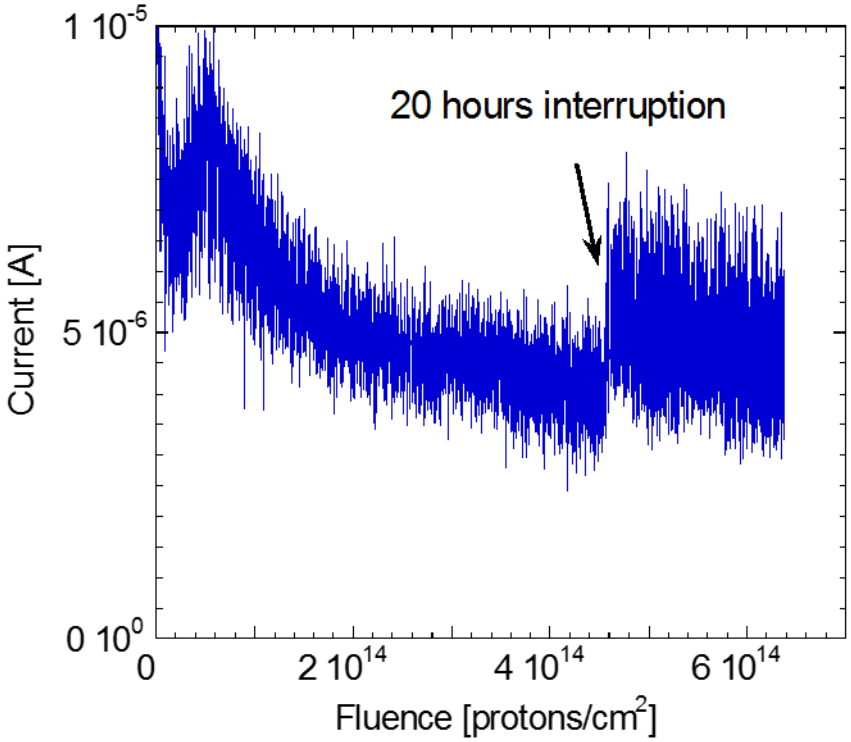

Figure 6: Current induced by the 24 GeV proton spills on a 32.6-µm-thick a-Si:H diode as a function of proton fluence within the CERN IRRAD1 facility. During the beam interruption at a fluence of 4.5×10^{14} protons/cm^2, the sample was kept under the same reverse bias voltage (300 V). The noise visible during the experiment originates from the variation of the beam intensity from spill to spill.

An in-depth understanding of the effect of irradiation on a-Si:H is still missing. Characterisation in terms of defect density or defect distribution is very incomplete due to difficulties to perform this type of investigation on a-Si:H in general and on radioactive sample (after irradiation) in particular. While the influence of the type of particle and its energy on the material or diode properties can be deduced from various studies found in the literature, the evolution of those properties with time as a function of the irradiation history cannot yet be forecasted with enough confidence.

3. Vertically integrated a-Si:H detectors

Because of its performance as a particle detector and its high radiation resistance, a-Si:H may be attractive for medical imaging, in addition to particle tracking in high-energy physics experiments. For these applications, vertically integrated a-Si:H detectors were fabricated following an approach pioneered by the University of Siegen for visible light imagers [73]. This approach, known as “thin film on ASIC” (TFA) or “thin film on CMOS” (TFC), consists in a vertical integration of the detecting layer on top of the readout electronics. It is obtained by the

direct deposition of an a-Si:H diode layer stack on the CMOS readout chip (see Figure 7). The back electrodes (in general, the pads present on the readout chip) define the active area and the individual diodes. Such a monolithic device facilitates the integration of the detector with the readout electronics, reduces the related noise and can almost eliminate dead areas between pixels. TFA sensors were successfully developed, aiming at the detection of singly charged particles (including MIPs) and X-rays [74,75,76,77]. Examples of TFA detectors are shown in Figure 8. Successful detections of β particles from ^{63}Ni (with a maximum energy of 67 keV) and of beta particles from ^{90}Sr (with a maximum energy of 546 keV) were achieved as seen in Figure 9 [76].

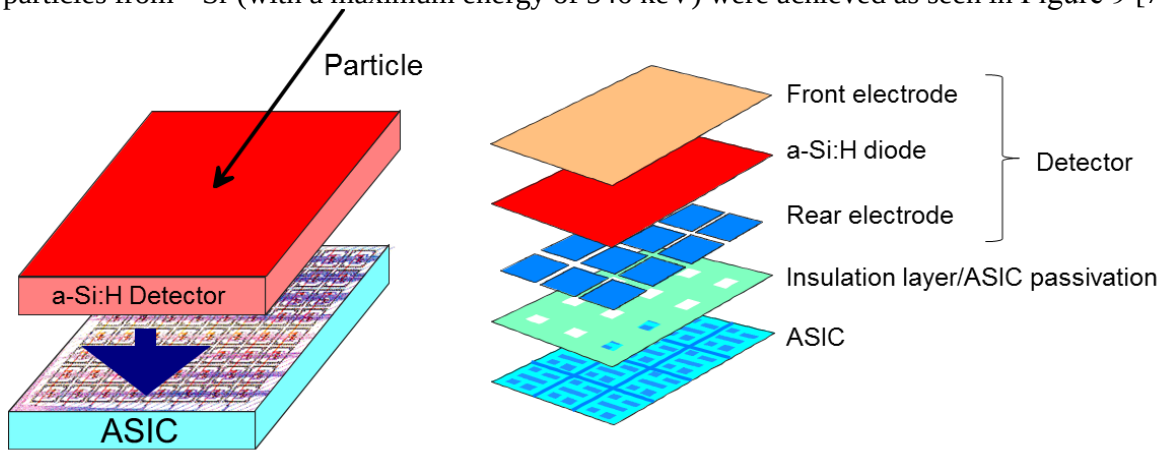

Figure 7: Schematic view of a thin film on ASIC (TFA) particle detector.

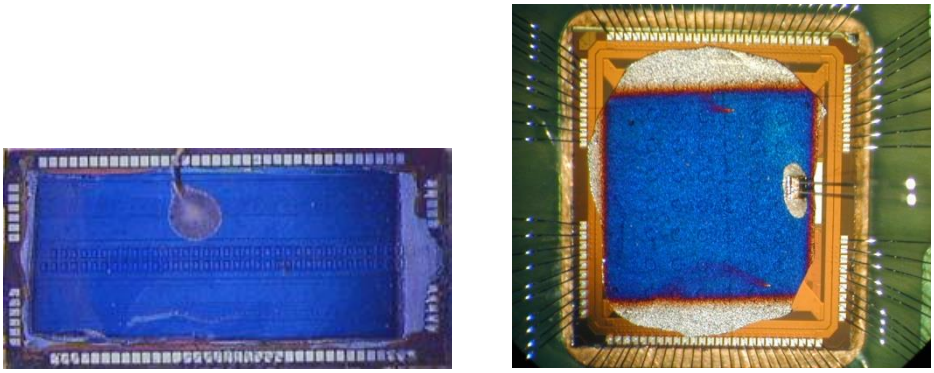

Figure 8: Photographs of (left) an "AFP chip" with a linear array of 32 pixels (only one row of the central pixels is used) consisting of a 32-µm-thick a-Si:H diode connected to an active feedback preamplifier (AFP) and (right) of a 8×6 pixel particle detector in TFA technology with a 15-µm-thick a-Si:H diode array. Each octagonal pixel has a lateral size of 150 µm with a pitch of 380 µm and is connected to an AFP and shaper. The top common Indium tin oxide (ITO) electrode is connected with a wire glued with Ag paste (left) or with a wire bonded to a gold tab glued with Ag paste.

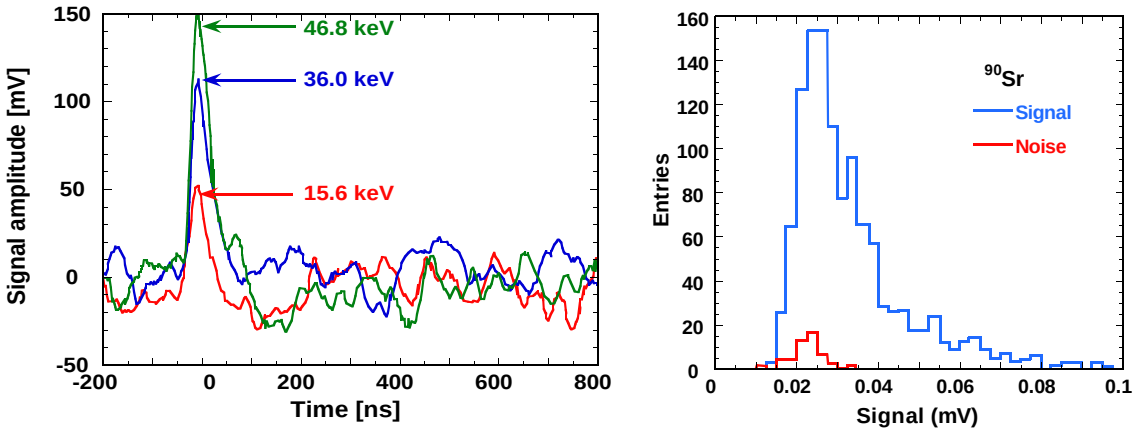

Figure 9: Signal as a function of β energy recorded with a ^{63}Ni β source (left) and distribution of amplitudes obtained with a ^{90}Sr β sources (right) with a 32-µm-thick TFA "AFP chip".

During the development of TFA imagers, it was observed that chip surface morphology and pixel geometry can affect the leakage current of the pixels [78]. A test chip was designed by CERN to study the effect of pixel geometry and edges on the performance of TFA sensors [79]. This chip included pixels of various sizes and shapes, micro-strips of various width and pitch values and two different geometries for the openings in the passivation layer of the chip. As for most TFA devices, the back contacts of the individual pixels are provided by the top metal layer of the ASIC through openings in the ASIC passivation. These openings can be local (for a single pixel) or global (for a group of pixels or the entire chip). The local openings correspond to the size of the metal pads, but can be slightly larger or smaller than the pads. For the TFA imagers [78], the edge of the passivation openings has a detrimental effect and may lead to large additional leakage. A global opening is therefore necessary to keep low leakage current values [79,80]. Diodes without an n-layer (i.e. an i-p layer structure deposited directly on the metallic back contact, metal-i-p configuration) even further reduce the leakage current [78,80].

The same test chip was also used to study spatial response and carrier collection as a function of diode and micro-strip geometries. From electron-beam-induced current (EBIC) measurements, lateral charge collection can be evaluated. For a-Si:H, lateral collection extends to only a few microns, as transport is driven mainly by drift. Micrometre-size high spatial resolution can therefore be achieved using pixelated devices or micro-strips [81]. Figure 10 shows an EBIC image of a set of micro-strips connected in parallel covered with a 5-µm-thick a-Si:H n-i-p diode. Each micro-strip (1.5 µm wide and spaced by 3.5 µm) is clearly resolved. Almost no cross-talk between micro-strips located only 4 µm apart was observed in another experiment with a radioactive beta source [79]. In contrast to c-Si based tracking devices where position is determined by the charge sharing between neighbouring channels, spatial resolution is here essentially determined by the shape of the a-Si:H diode electrodes. With limited lateral charge collection devices with feature size and pitch smaller than the diode thickness (typically of less than 20 µm) can be fabricated with almost no dead area. a-Si:H-based detectors could therefore be applied to beam or particle tracking with a resolution of a few microns.

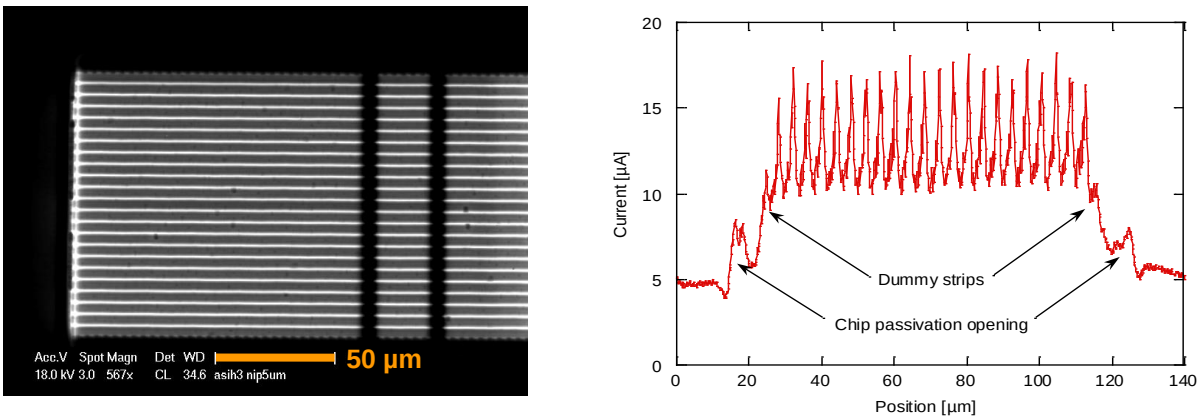

Figure 10: (Left) EBIC image of a set of micro-strips with a width of 1.5 µm and spacing of 3.5 µm covered with 5-µm-thick a-Si:H n-i-p diode and (right) corresponding signal from EBIC line scans through the micro-strip set. Measurement was performed at an applied voltage of 30 V and beam energy of 20 keV. All strips are connected in parallel. The two vertical dark bands in the EBIC image correspond to areas degraded by previous EBIC line scans.

As observed for a-Si:H particle detectors deposited on glass, full depletion was here also difficult to attain in diodes thicker than 15 µm. This thickness value seems for the time being to be an optimal value in terms of ease of fabrication and depletion region width [79]. The maximum signal-to-noise ratio was on the order of 5 (higher than previous results from detectors deposited on glass) which is still insufficient for clear single MIP detection [79,82]. However, as discussed in the previous section a clear room for improvement of this noise-to-signal ratio exists. Optimizing the growth of the material for low defect density (deposition using low growth rates such as the ones used for state-of-the-art solar cell fabrication – with a reduction of the growth rate by at least a factor of 10 with respect to the one used for the present detectors) could reduce the defect density by up to one order of magnitude and could then allow for much thicker device with full depletion. Such deposition conditions at low rates have not yet been considered as they substantially increase the processing time and result in more dense and mechanically stressed layers (requiring additional optimization to avoid layer delamination). Optimization of the device p-i interface for low leakage current and deposition of the detector on a readout chip with a flat surface morphology are also proven solutions which permit higher device thicknesses and bias electric field values without increasing the leakage current. These two approaches (separately of jointly) should enable a higher signal-to-noise ratio, possibly allowing for clear single MIP detection.

4. Detectors using an indirect detection scheme

The combination of a Si detector with a scintillating layer can be used to avoid the limitations of Si to detect MIPs. Such a detection scheme has been successful for X-ray radiography using a-Si:H photodiodes [83,84,85]. With the ability of a-Si:H to be deposited on large areas, X-ray imagers of various sizes have been developed and deployed for medical applications. These imagers comprise a thin-film transistor (TFT) backplane used to address the individual a-Si:H photodiodes, which are integrated on the same substrate as the TFTs. A scintillating layer such as CsI is deposited on top of the photodiode array. Readout is performed by sequentially addressing each row of photodiodes, switching on the respective TFTs and extracting the collected charge stored on these photodiodes. Benefiting from the possibility to deposit a-Si:H on large substrate, large-area X-ray imagers able to perform chest radiography, for example, have been developed [86]. Besides radiography, such imagers can also be used for other types of medical imaging such as fluoroscopy and angiography, reducing the X-ray dose for the patient [87]. While MIP detection can be performed with large-area devices, their application and design is for imaging and they are not capable of single MIP detection. Detection is here limited by the TFT leakage, readout frequency and imager size.

Positron emission tomography (PET) scanning [88] is also attracting attention for the application of a-Si:H photodiodes [89]. This medical imaging technique is based on the use of a radioactive positron emitter injected into the patient's blood. Shortly after the emission, the positron annihilates itself with a nearby electron leading to the emission of two 511 keV photons in opposite directions. A synchronous detection is required to reconstruct the emission region. For this purpose, fast-decaying scintillating materials are needed. Within the Crystal Clear Collaboration [90], several fast scintillators have been developed and studied. However, most have their peak emission at UV or deep blue wavelengths, which are more difficult to record using a-Si:H photodiodes [89]. However, a-Si:H n-i-p photodiodes with thinner p-doped layers and an optimized front transparent electrode (transparent conductive oxide, TCO), or photodiodes in the reverse configuration (p-layer at the back with respect to illumination) without an n-layer, can achieve high external quantum efficiency at wavelengths of interest, as shown in Figure 11. While an integrated device combining a fast scintillator, a-Si:H diodes and readout electronics has not yet been tested, the performance of the individual components seems sufficient to allow for gamma detection in PET scanners [89].

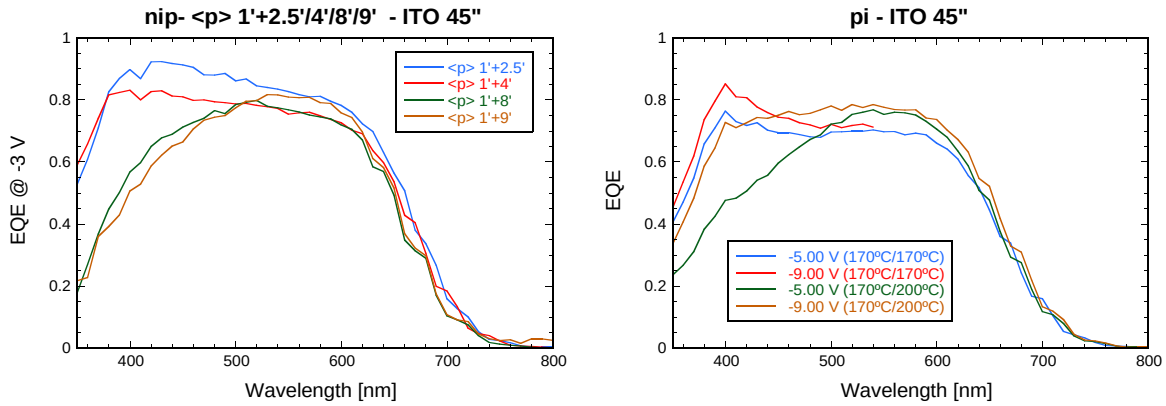

Figure 11: External quantum efficiency (EQE) of several a-Si:H diodes: (left) in the metal-n-i-p-TCO configuration with various p-layer thickness and (right) in the metal-p-i-TCO configuration. The p-layer is formed of a stack of two individual layers: the first one is the same for all diodes (1' deposition time) while the deposition time, and thickness, of the second layer are variable. Indium tin oxide (ITO) is used here as the TCO layer.

An innovative particle detector using an indirect detection scheme was recently proposed. It comprises a microfluidic device filled with a scintillating liquid where the microchannels are also used to guide the light to the photodiodes [91]. a-Si:H is attractive for this application, as photodiodes can be deposited directly on the microfluidic device for monolithic integration. Also in this case the device geometry, light yield of the scintillating liquid and light propagation through the micochannels should not allow for single MIP detection when combined with a-Si:H photodiodes. Applications to beam monitoring are nevertheless possible [92].

5. a-Si:H-based microchannel plate detectors (AMCP)

5.1 AMCP concept

Microchannel plates (MCPs) are electron-multiplier devices [93] that were initially developed for night vision [93] and astrophysics applications [94,95] and then used in a variety of other fields. Such detectors consist in thick glass plates with very narrow microchannels (or pores) drilled throughout the device. When a primary electron hits the channel wall, secondary electrons are emitted. Since a high electric field is applied between the two faces of the plate, the primary electrons multiply by impact ionization forming an avalanche within the microchannels. A schematic view of such a device and its functioning is shown in Figure 12. Gains in excess of 1000 can be achieved from a single plate. To enhance the gain, microchannels are not perpendicular to the surface but at a certain angle (referred as bias angle). Much higher values are obtained when

stacking several devices in a chevron arrangement [**Error! Bookmark not defined.**]. When combined with a low-noise readout chip, detection of MIPs can be achieved. State-of-the-art MCPs are fabricated from lead glass, and the channel walls are coated with a conductive material to ensure charge replenishment.

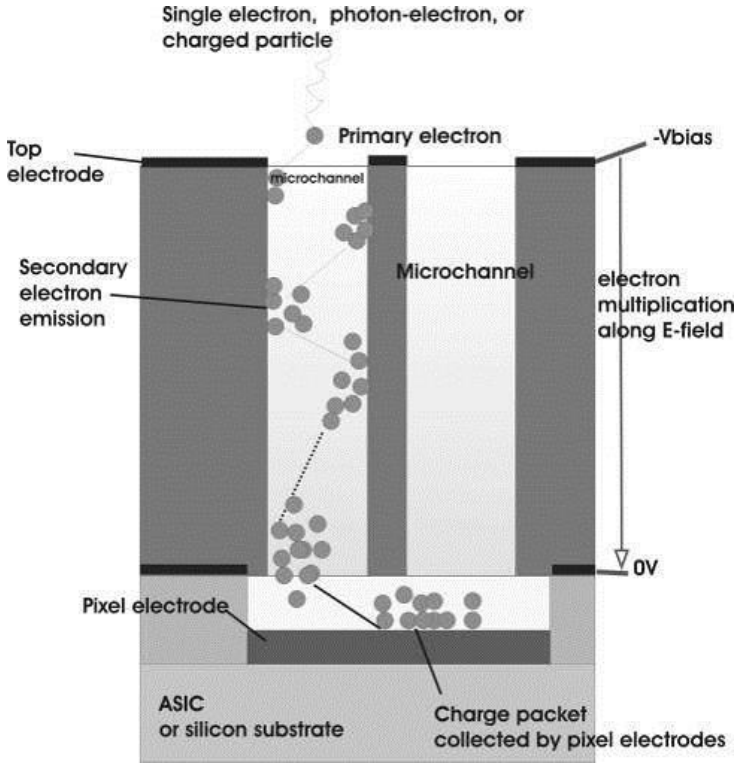

Figure 12: Schematic cross section of two channels of a MCP device stacked on a readout electronic chip.

We recently proposed MCP detectors based on a-Si:H as an alternative to particle detection using thick diodes [96,97]. The properties of a-Si:H could overcome some of the limitations introduced by the lead glass or the c-Si usually used for MCP fabrication [98,99]. The bulk resistivity of a-Si:H (see section 1.2) is high enough to sustain a high bias voltage and small enough to provide charge replenishment after the emission of secondary electrons while keeping reasonably low leakage current and to avoid the need of coating the channel walls for charge replenishment. With a more efficient charge replenishment along the length of the channel, a-Si:H-based MCPs (AMCPs) are expected to have much shorter dead time (time needed for charge replenishment) and larger gain under continuous operation.

Another key advantage of AMCPs is the possibility to vertically integrate MCPs on the readout electronics, similar to the approach used for TFA detectors (see section 3). All fabrication steps are at processing temperatures ≤200°C (see below) and fully compatible with CMOS electronics. Such monolithic integration should provide low noise and low power consumption and ease single MIP detection. An additional advantage of AMCPs is that channel micromachining is performed using deep reactive ion etching (DRIE), which allows the channel geometry to be fully customized and adapted to the readout electronics. The combination of photolithography and DRIE can provide aspect ratios comparable to lead-glass MCPs [100].

5.2 AMCP fabrication

All AMCPs thus far were fabricated on thermally oxidized Si wafers (500 μm thick, single or double side polished) with patterned Al or Cr electrodes. This substrate was chosen to mimic as

much as possible the device structure of a fully integrated AMCP on its readout electronics. The main part of the AMCP consists in a thick (up to 120 µm) a-Si:H layer covered with a doped a-Si:H layer used as the top electrode. After the deposition of the layer stack, a first patterning/etching step is performed to define the individual device (test reticles) and to uncover the bonding pads, followed by the DRIE step to drill the microchannels. The critical aspects of the fabrication reside primarily in the deposition of the thick a-Si:H layer. This is performed by PE-CVD (as for other a-Si:H devices) under conditions that must minimize stress in the layer to avoid delamination of the stack or formation of blisters. Details on the fabrication can be found in [101] and [102].

The first generation of AMCPs consisted in simple two-terminal devices: a bottom electrode deposited on the oxidized wafer and a top doped layer. While avalanche events could be demonstrated using EBIC measurements [97], this configuration did not allow us to separate the current induced by the avalanche from the leakage current through the AMCP structure. A new generation was designed featuring an additional electrode at the back, separated from the bottom readout electrode (anodes) by a thin insulating layer [101]. The overall device structure and detailed scanning electron microscope (SEM) images of the device are given in Figure 13. In this configuration, the bias electric field used to induce avalanches and electron multiplication is applied between the top and intermediate electrode, while the bottom electrode is used for readout and is therefore insulated from the leakage current. In the same figure, detailed SEM images from the channel entrance and bottom of the channel are also presented.

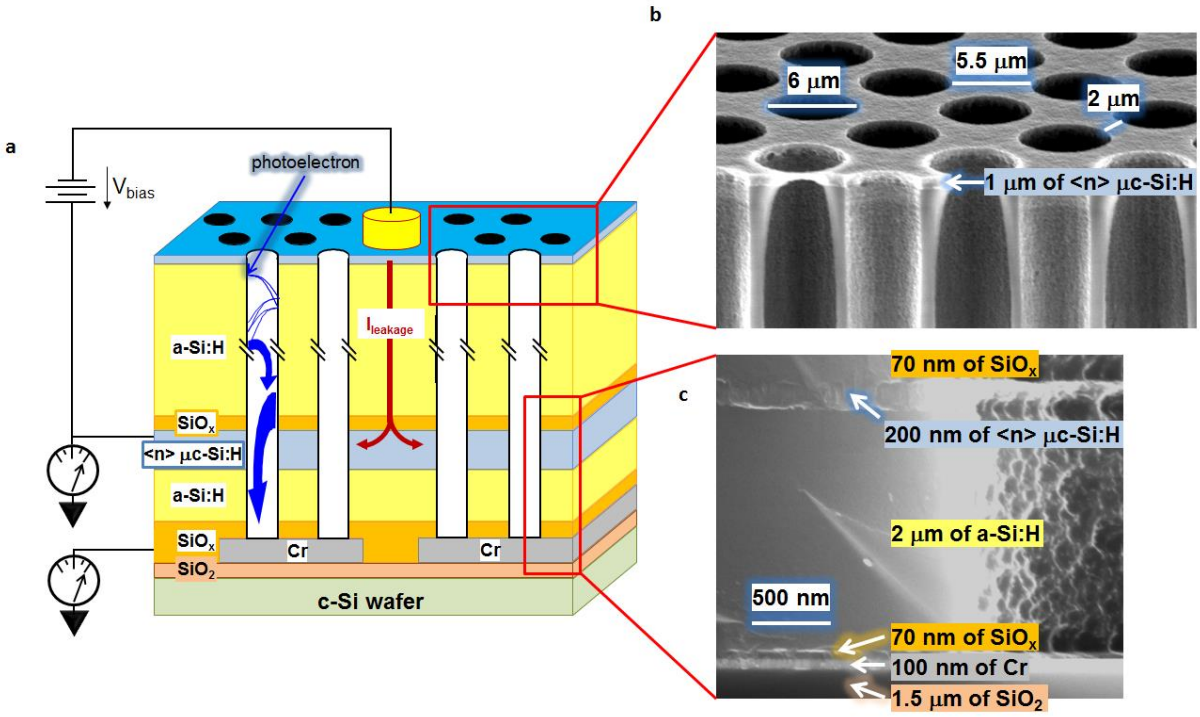

Figure 13: (a) Schematic view of a vertically integrated AMCP on chromium readout anodes. The electric field for electron multiplication is applied between the top and intermediate electrodes. (b) SEM image of the AMCP channel openings and (c) of the intermediate and bottom readout electrodes separated by an insulating layer stack. From [101].

AMCPs with channel lengths of up to 100 µm have been fabricated with a variety of microchannel diameters (or channel apertures) between nominally 4 and 6 µm. Microchannels with parallel walls could be obtained for all geometries; however, DRIE led to a slight increase in the channel aperture (by 1 to 1.5 µm from the nominal diameter). Aspect ratio values of up to 15 were demonstrated.

5.3 AMCP performance

AMCP devices were characterized by means of EBIC measurements and in quasi-steady state mode with electron irradiation from a photocathode illuminated by UV light. Excitation was here modulated by chopping the illumination at low frequency (< 1 kHz). Gain was obtained from the difference between the signals with and at 0 V bias voltage applied. Comparisons of the gain for different channel geometries (effect of channel length and aspect ratio) are plotted in Figure 14.

At this stage the observed gain values and their dependency on channel geometry is consistent with the performance observed in state-of-the-art lead-glass MCPs. According to the model developed by Eberhardt [103], we could expect the gain values of AMCPs to increase by a factor of 10^2–10^3 for an aspect ratio of 30, a value which is achievable with DRIE of Si [104]. From the modelling of the present AMCP, a secondary electron yield – the number of electrons generated per collision – of 1.5–1.7 was inferred. This yield (and, as a consequence, the AMCP gain), which is quite low compared to values achieved in state-of-the-art photomultiplier tube dynodes (values of 4), should be increased by coating the channel wall with Al_2O_3 as done in state-of-the-art MCPs [105]. A first test with such a coating in an AMCP led to an increase of the gain by a factor of 2 [102]. Possible alternatives to explore are SiO_2, Si_3N_4 [106] or diamond-like layers [107].

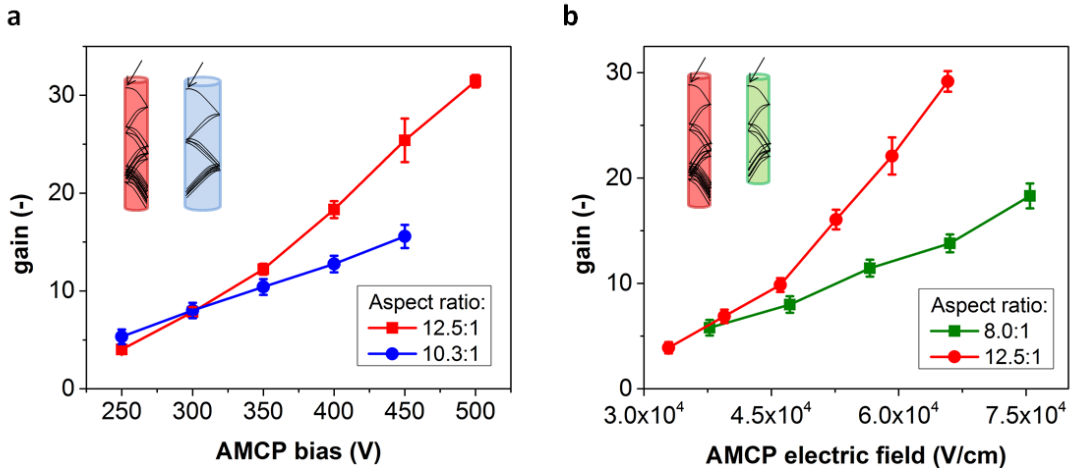

Figure 14: AMCP gain dependency on aspect ratio. (a) Gain versus bias voltage for aspect ratios of 10.3:1 and 12.5:1, with a channel length of 76 µm and channel apertures of 7.6 and 6.1 µm, respectively. (b) Gain versus electric field for aspect ratios of 12.5:1 and 8:1, with a channel aperture of 6.1 µm and channel lengths of 76 and 53 µm, respectively. From [101].

By increasing the aspect ratio of AMCPs to values around 30 and improving the secondary emission yield (with an optimized coating), gain values approaching10^4 can be expected. With a vertical integration of AMCPs on low-noise readout electronics, the detection of a single MIP should be possible at very high repetition rate. Nevertheless, besides the demonstration of such gain values, a comprehensive analysis of AMCPs is still to be carried out. As observed during the development of AMCPs, AMCPs exhibit drift of their performance (marked reduction of the gain) under steady-state operation (AMCP continuously exposed to electrons emitted from a photocathode). While a charging effect of the SiO_x layers present in the layer stack has been observed, the metastability of the material (see section 1.2) could also be involved. Finally no performance analysis in transient and low excitation conditions (towards single particle detection) has yet been completed.

6. Future prospects and conclusions

While a-Si:H-based detectors have been successfully deployed for digital radiography, they have not (yet) found their place in other applications. Despite the attractive features of a-Si:H, such as large-area deposition, relatively easy processing and high radiation resistance, the difficulty to achieve a high signal-to-noise ratio for MIP detection and the unclear benefits of this technology

compared to other materials have discouraged most of the actors. The performance of the devices fabricated in our laboratory or reported in the literature is clearly not at the level of what could be possible. This is not too surprising given the much smaller effort invested for particle-detection applications compared to the effort invested for solar cell or transistor applications. The need for thick devices also adds more difficulties in the mastering of the technology. Diode leakage current could be reduced by an improvement in material quality and diode design. The design and fabrication of CMOS chips dedicated to TFA would also permit a gain in performance.

The very high spatial resolution of a-Si:H permitted by TFA technology has not yet been exploited. This resolution is basically given by the geometry of the back electrode(s) of the diode and could be as small as a few micrometres. High-precision beam positioning, beam shaping or particle tracking/imaging could be achieved with this technology.

Indirect detection using scintillators could possibly achieve single MIP detection. Application to PET scanners was targeted by a few groups but little effort has been invested and little progress made for any successful application. New detector concepts using scintillating liquid and microfluidic devices offer new perspectives, but the detection volume strongly reduces the number of available photons and completely prohibits single MIP detection. However the technology could allow for flexible devices or geometries that are not achievable by other means and thus could possibly initiate new applications.

MCPs are an exciting new application of a-Si:H. Achieving single particle detection by improving the gain would pave the way for many applications. Vertical integration on readout electronics developed for nuclear physics (such as Medipix or NINO chips) would allow for photon-counting imagers. AMCPs could be applied to a wide range of applications that need both a high spatial resolution (given by the pitch of the microchannel) and ultra-fast time resolution. Comprehensive studies are still needed to understand the material behaviour in AMCP and the fundamental limits of its operation. Furthermore the gain is still too low and must be improved by at least an order of magnitude to permit any practical application.

The potential for a-Si:H-based detector deployment remains considerable as the requirements for radiation-resistant detectors become more stringent. An increase in the luminosity of modern accelerators is calling for alternative solutions for the detectors. There are several candidates that could offer the required properties. However, all materials have benefits and drawbacks, and a-Si:H is no exception.

Acknowledgments

Part of the results presented were obtained with the financial support of CERN, ETHZ and of the Swiss National Science Foundation projects 126926/1 and 144375/1.

Appendix. List of abbreviations

a-Si:H	Hydrogenated amorphous silicon
AFP	Active feedback amplifier
AMCP	a-Si:H-based MCP
ASIC	Application-specific integrated circuit
CMOS	Complementary metal-oxide semiconductor
CVD	Chemical vapour deposition
DB	Dangling bond
DRIE	Deep reactive ion etching
EBIC	Electron-beam induced current
e-h	electron-hole
ITO	Indium tin oxide
LHC	Large Hadron Collider
MCP	Microchannel plate (detectors)
MIP	Minimum ionizing particle
SEM	Scanning electron microscope

TCO	Transparent conductive oxide
TFA	Thin film on ASIC
TFC	Thin film on CMOS
TFT	Thin-film transistor
UV	Ultraviolet

References

[1] Milbrath B D Peurrung Bliss M Weber W J 2008 Radiation detector materials: An overview *J. Mater. Res.* 23 2561-2581

[2] Casse G 2013 Recent developments on silicon detectors *Nucl. Instr. and Meth. in Phys. Res.* A732 16–20.

[3] Chittik R C Alexander J H Sterling H E 1969 The Preparation and Properties of Amorphous Silicon *J. Electrochem. Soc.* 116 77-81.

[4] Fritzsche H 1980 Characterization of Glow-Discharge Deposited a-S:H *Sol. Ener. Mat.* 3 447-501

[5] Spear W Lecomber P G 1976 Electronic properties of substitutionally doped amorphous Si and Ge *Phil. Mag.* 33 935-949

[6] Tuan H C 1984 Amophous Silicon Thin Film Transistor and its Application s to Large-Area Electronics *Mater. Res. Soc. Proc.* 33 247

[7] Carlson D E Wronski C R 1976 Amorphous silicon solar cell *Appl. Phys. Lett.* 28 671-673

[8] Owen A E Le Comber P G Spear W E Hajto J 1983 Memory switching in amorphous silicon devices *J. of Non-Cryst. Sol.*59-60 1273–1280

[9] Rech B Wagner H 1999 Potential of amorphous silicon for solar cells *Appl. Phys.* A 69 155-167

[10] Rech B Wieder S Siebke F Beneking C Wagner H 1966 Material Basis of Highly Stable a-Si:H Solar Cells *Mater. Res. Soc. Symp. Proc.* 420 33

[11] Shah S Dutta J Wyrsch N Prasad K Curtins H Howling A Hollenstein C 1992 VHF plasma deposition: A comparative study *Mater. Res. Soc. Proc.* 258 15-26

[12] Paquin L Masson D Wertheimer M R Moisan M 1985 Amorphous silicon for photovoltaics produced by new microwave plasma-deposition techniques *Canadian Journal of Physics* 63 831-837

[13] Mahan A 2003 Hot wire chemical vapor deposition of Si containing materials for solar cells *Sol. Ener. Mat. and Sol. Cells* 718 299-327

[14] Wronski C R Lee S Hicks M Kumar S 1989 Internal photoemission of holes and the mobility gap of hydrogenated amorphous silicon *Phys. Rev. Lett.* 63 1420-1423

[15] Tauc J Grigorovici R Vancu A 1966 Optical properties and electronic structure of amorphous germanium *Phys. Stat. Sol.* (b) 15 627-637

[16] Zanzucchi P Wronski C R Carlson D E 1977 Optical and photoconductive properties of discharge-produced amorphous silicon *J. of Appl. Phys.* 48 5227-5236

[17] Smets A H M Kessels W M M van de Sanden M C M 2003 Vacancies and voids in hydrogenated amorphous silicon *Appl. Phys. Lett.* 82 1547-1549

[18] Smets A H M Wronski C R Zeman M van de Sanden M C M 2010 The Staebler-Wronski Effect: New Physical Approaches and Insights as the Route to Reveal its Origin *Mater. Res. Soc. Symp. Proc.*, 1245 A.14.02

[19] Lee Y Jiao L Liu H Lu Z Collins R Wronski C W 1996 Stability of a-Si:H solar cells and corresponding intrinsic materials fabricated using hydrogen diluted silane *Proc. of the 25th IEEE photovolt. Spec, conf.*, pp 1165-1168
[20] Kondo M Matsuda A 2002 An approach to device grade amorphous and microcrystalline silicon thin films fabricated at higher deposition rates *Curr. Opinion in Solid State and Mat. Sci.* 6 445–453
[21] Roca i Cabarrocas P Fontcuberta i Morral A Poissant Y 2002 Growth and optoelectronic properties of polymorphous silicon thin films *Thin Solid Films* 403 39-46
[22] Street R A 1982 Doping and the Fermi energy in amorphous silicon *Phys. Rev. Lett.* 49 1187-1190
[23] Staebler D L Wronski C W 1977 Reversible conductivity changes in discharge-produced amorphous Si *Appl. Phys. Lett.* 31 292-294
[24] Kolodziej A 2004 Staebler-Wronski effect in amorphous silicon and its alloys *Opto-Electron. Rev.* 12 21-32
[25] Stradins P 2010 Staebler-Wronski Defects: Creation Efficiency , Stability, and Effect on a-Si:H Solar Cell Degradation *Proc. of the 25th IEEE photovolt. Spec. Conf.* pp 142-145
[26] Street R A 2005 *Hydrogenated Amorphous Silicon* (Cambridge, Cambridge University Press)
[27] Shah A 2010 *Thin-Film Silicon Solar Cells* (Lausanne, EPFL Press)
[28] Paduschek P Höpfl C Mitlehner H 1983 Hydrogen-Related Mechanical Stress in Amorphous and Plasma-deposited Silicon Nitride *Thin Solid Films* 110 291-304
[29] Kroll U Meier J Shah A Mikhailov S Weber J 1996 Hydrogen in amorphous and microcrystalline silicon films prepared by hydrogen dilution *J. of Appl. Phys.* 80 4971
[30] Chabloz P Keppner H Fischer D Link D Shah A 1996 Amorphous silicon p-i-n diodes, deposited by the VHF-GD process: new experimental results *J. of Non-Cryst. Sol.* 198-200 1159
[31] Wyrsch Miazza C Ballif C Shah A Blanc N Kaufmann R Lustenberger F Jarron P 2005 Vertical integration of hydrogenated amorphous silicon devices on CMOS circuits *Mater. Res. Soc. Proc.* 869 3-14
[32] Leo W R 1994 Passage of Radiation Through Matter *Techniques for Nuclear and Particle Physics Experiments* (Berlin, Springer-Verlag) pp 17-68
[33] Wyrsch N *et al.* 2003 Development of Vertically Integrated Imaging and Particles Sensors *Mater. Res. Soc. Proc.* 762 205
[34] Pochet T Dubeau J Equer B Karar A Hamel L A 1990 High reverse voltage amorphous silicon p-i-n diodes *J. of Appl. Phys.* 68 1340-1344
[35] Fujieda I *et al.* 1990 Field Profile Tailoring in a-Si:H Radiation Detectors *Mat. Res. Soc. Symp. Proc.* 192 399-404
[36] Perez-Mendez V *et al.* 1991 Amorphous Silicon Based Radiation Detectors *J. of Non-Cryst. Sol.* 137-138 1291-1296
[37] Morrison S Servati P Vygranenko Y Nathan A Madan A 2002 Reduction of Dark Current Under Reverse Bias in a-Si:H p-i-n Photodetectors *Mat. Res. Soc. Symp. Proc.* 715 701
[38] van der Graaf H 2010 Gaseous detectors *Nucl. Instr. and Meth. in Phys. Res.* A 628 27-30
[39] van der Graaf H et al. 2013 The gridpix detector: History and perspective *Mod. Phys. Lett.* A 28 1-7.
[40] Perez-Mendez V Morel J Kaplan S N Street R A 1986 Detection of Charged Particles in Amorphous Silicon Layers *Nucl. Instr. and Meth. in Phys. Res.* 252 478-482

[41] Perez-Mendez V Kaplan S N Ward W Qureshi S Street R A 1987 Signal, Recombination Effects and Noise in Amorphous Silicon Detectors *Nucl. Instr. and Meth. in Phys. Res.* A260 195-200
[42] Perez-Mendez V Kaplan S N Cho G Fujieda Qureshi S Ward W Street R A 1988 Hydrogenated Amorphous Silicon Pixel Detectors for Minimum Ionizing Particles *Nucl. Instr. and Meth. in Phys. Res.* A273 127-134
[43] Xi J *et al.* 1991 Minimum ionizing particle detection using amorphous silicon diodes *Nucl. Instr. and Meth. in Phys. Res.* A301 219-222
[44] Equer B Karar A 1988 Effect of Primary Ionization in Amorphous Silicon Detectors *Nucl. Instr. and Meth. in Phys. Res.*A271 574 584
[45] Hordequin C Brambilla Bergonzo P Foulon F 2001 Nuclear radiation detectors using thick amorphous-silicon *Nucl. Instr. and Meth. in Phys. Res.* A456 284-289
[46] Aglietti U Bacci C Evangelisti F Falconieri M Fiorini P Meddi F 1989 a-Si:H p-i-n Junction as Ionizing Particle Detectors *J. of Non-Cryst. Sol.* 115 177-179
[47] Kishimoto N Amekura H Kono K LeeC G 1998 Stable photoconductivity in metastable a-Si:H under high-energy proton irradiation *J. of Non-Cryst.* Sol. 227-230 238-242.
[48] Chabloz P *et al.* 1992 X-Ray Detectors Based on "Thick" a-Si:H Layers Deposited by the VHF-GD Process *Mater. Res. Soc. Proc.* 258 1057-1062
[49] Aleksan R Bolognese T Equer B Karar A Reymond J M 1991 Observation of single minimum ionising particles with amorphous silicon diodes *Nucl. Instr. and Meth. in Phys. Res.* A305 512-516
[50] Dubeau J Pochet T Hamel L A Equer B Karar A 1991 Response of amorphous silicon p-i-n detectors to ionizing particles *Nucl. Instr. and Meth. in Phys. Res.* B54 458 471
[51] Klein C A 1968 Bandgap Dependence and Related Features of Radiation Ionization Energies in Semiconductors *J. of Appl. Phys.* 39 2029-2038 *IEEE Trans. Nucl. Sci.* 36 1347-1352
[52] Naruse Y Hatayama T 1989 Metal/amorphous Silicon Multilayer Radiation Detectors
[53] Caracciolo H, Balbinot G, Bazzano G, Bosser J, Caldara M, Parravicini A, Pullia M, Viviani C 2011 Beam Diagnostics Commissioning at CNAO *Proc. of the 2nd Int. Particle Accelerator Conf.* (IPAC2011) pp 2848-2850
[54] Hong W S *et al.* 1995 Charged particle detectors based on high quality amorphous silicon deposited with hydrogen or helium dilution of silane", *IEEE Trans. Nucl. Sci.* 42 240-246
[55] Quereshi S Perez-Mendez V Kaplan S N Fujeda I Gho G Street R A 1989 Material Parameters in Thick Hydrogenated Amorphous Silicon Radiation Detectors *J. of Non-Cryst. Sol.* 114 417-419
[56] Pochet T Illie A Foulon F Equer B 1994 Characterization of new a-Si:H Detectors fabricated fiom Amorphous Silicon deposited at High Rate by Helium enhanced PECVD *IEEE Trans. on Nucl. Sci,* 41 1014 1018
[57] Despeisse M *et al.* 2008 Hydrogenated Amorphous Silicon Sensor Deposited on Integrated Circuit for Radiation Detection. *IEEE Trans. on Nucl. Sci.* 55 802-811
[58] Morasanu C *et al.* 1993 a-Si:H based particle detectors with low depletion voltage *J. of Non-Cryst. Sol.* 164-166 801-804.
[59] Perez-Mendez V Cho G Fujieda I Kaplan S N Qureshi S Street R A 1989 The Application of Thick Hydrogenated Amorphous Silicon Layers to Charge Particle and X-ray Detection *Mater. Res. Soc. Proc.* 149 621-630
[60] Mireshghi A *et al.* 1994 High Efficiency Neutron Sensitive Amorphous Silicon Pixel Detectors *IEEE Trans. on Nucl. Sci.* 41 915 921

[61] Foulon F Bergonzo P Brambilla C Jany C Guizard B Marshall R D 1998 Neutron Detectors Made from Chemically Vapour Deposited Semiconductors *Mater. Soc. Res. Proc.* 487 591-
[62] Antonuk L E Boudry J Yorkston J Wild C F Long M J Street R A 1990 Radiation damage studies of amorphous-silicon photodiode sensors for applications in radiotherapy X-ray imaging *Nucl. Instr. and Meth. in Phys. Res.* A 299 143-146
[63] Srour J R Vendura G J Lo D H Toporow C M C Dooley M Nakano R P King E E 1998 Damage Mechanisms in Radiation-Tolerant Amorphous Silicon Solar Cells *IEEE Trans. on Nucl. Sci.* 45 2624-2631
[64] Schwarz R Kolodzey J Alijishi S Wagner S 1985 Radiation Damage by 12 MeV Protons and Annealing of Hydrogenated Amorphous Silicon *Proc. of the 18th IEEE Photovolt. Spec. Conf.* 903
[65] Kuendig J Goetz M Shah A Gerlach L Fernandez E 2003 Thin film silicon solar cells for space applications: Study of proton irradiation and thermal annealing effects on the characteristics of solar cells and individual layers *Sol. Ener. Mat. & Sol. Cells* 79 425-438
[66] Boudry J M Antonuk L E 1994 Radiation Damage of Amorphous Silicon Photodiode Sensors *IEEE Trans. Nucl. Sci.* 41 703-707
[67] Bacci C *et al.* 1991 Detection of strongly ionizing particles with a hydrogenated amorphous silicon detector *Nucl. Instr. and Meth. in Phys. Res.* A306 182-186
[68] Bätzner D L Romeo A Terheggen M Döbeli M Zogg H Tiwari A N 2004 Stability aspects in CdTe/CdS solar cells *Thin Solid Films* 451–452 536–543
[69] Klaver A 2007 Irradiation-induced degradation of amorphous silicon solar cells in space , *TU Eindhoven Ph.D. Thesis* http://repository.tudelft.nl/file/768999/375461
[70] Wyrsch N *et al.* 2006 Radiation hardness of amorphous silicon particle sensors *J. of Non-Cryst. Sol.* 352 1797-1800
[71] Schneider U Schröder B Finger F 1987 The creation of metastable defects in a-Si:H films by high dose irradiation with keV-electrons *J. of Non-Cryst. Sol.* 97&98 795-798
[72] Diehl F Herbst W Bauer S. Schröder B Oechsner H 1996 Metastability in p- and n-type a-Si:H investigated by keV-electron irradiation *J. of Non-Cryst.* Sol. 198-200 436-440
[73] Schneider B Rieve P Böhm M Jähne B Haußecker H Geißler P 1999 *Handbook on Computer Vision an Applications* (Boston, Academic Press) pp 237-270
[74] Wyrsch N Miazza C Dunand D Shah A Moraes D Anneli G Despeisse M Jarron P Dissertori G Viertel G 2004 Vertically Integrated Amorphous Silicon Particle Sensors *Mater. Soc. Res. Proc.* 808 441
[75] Anelli G *et al.* 2004 A new concept of monolithic silicon pixel detectors: Hydrogenated amorphous silicon on ASIC *Nucl. Instr. and Meth. in Phys. Res.* A518 366-372
[76] Wyrsch N *et al.* 2004 Thin-film silicon detectors for particle detection *Physica Status Solidi* (c) 1 1284-1291
[77] Jarron P *et al.* 2006 TFA pixel sensor technology for vertex detectors *Nucl. Instr. Meth. in Phys. Res.* A560 122-126
[78] Miazza C *et al.* 2006 Image Sensors Based on Thin-film on CMOS Technology: Additional Leakage Currents due to Vertical Integration of the a-Si:H Diodes *Mater. Res. Soc. Proc. Symp.* 910 A17-03.
[79] Despeisse M Anelli G Kaplon J Moraes D Nardulli A Powolny F Wyrsch N 2008 Hydrogenated Amorphous Silicon Sensor Deposited on Integrated Circuit for Radiation Detection *IEEE Trans. Nucl. Sci.* 55 802-811

[80] Wyrsch N Choong G Miazza C Ballif C 2008 Performance and Transient Behavior of Vertically Integrated Thin-film Silicon Sensors *Sensors* 8 4656-4668
[81] Franco A Riesen Y Despeisse M Wyrsch N Ballif C 2012 High Spatial Resolution of Thin-Film-on-ASIC Particle Detectors *IEEE Trans. Nucl. Sci.* 59 2614-2621
[82] Moraes D *et al.* 2004 A novel low noise hydrogenated amorphous silicon pixel detector *J. of Non-Cryst. Sol.* 2004 729-731
[83] Kim H K Cunningham I A Yin Z Cho G 2008 *Int. J. of Prec. Engin. and Manuf.* 9 86-100
[84] Moy J-P 1999 Large area X-ray detectors based on amorphous silicon technology *Thin Solid Films* 337 213-221.
[85] Nathan A *et al.* 2000 Amorphous silicon detector and thin film transistor technology for large-area imaging of X-rays *Microelectronics J.* 31 883–891.
[86] Kroft L J M Veldkamp W J H Mertens B J A Boot M V Geleijns J 2005 Comparison of Eight Different Digital Chest Radiography Systems: Variation in Detection of Simulated Chest Disease Amer. *J. of Roentgenology* 185 339-346
[87] Spahn M 2005 Flat detectors and their clinical applications *Eur Radiol*. 15 1934–1947
[88] Peng H Levin C S 2010 Recent Developments in PET Instrumentation *Curr Pharm Biotechnol.* 11 555–571
[89] Nardulli A *et al.* 2008 Quantum efficiency measurement of n–i–p a-Si:H photodiode arrayon CMOS circuit for positron emission tomography (PET) *J. of Non-Cryst. Sol.* 354 2603–2605
[90] http ://crystalclear.web.cern.ch
[91] Mapelli A *et al.* 2010 Scintillation particle detection based on microfluidics *Sensors and Actuators* A162 272–275
[92] Maoddi P 2015 Microfluidic Scintillation Detectors for High Energy Physics *EPFL PhD thesis* 6620
[93] Wiza J L 1979 Microchannel plate detectors *Nucl. Instr. and Meth. in Phys. Res.* 162 587-601
[94] Siegmund O, Malina R, Coburn K, Werthimer D 1984 Microchannel plate EUV detectors for the Extreme Ultraviolet Explorer *IEEE Trans. Nucl. Sci.* 31 776-779
[95] Fraser G, Barstow M, Whiteley M, Wells A 1982 Enhanced soft x-ray detection efficiencies for imaging microchannel plate detectors *Nature* 300 509-511
[96] Powolny F 2009 Characterization of time resolved photodetector systems for Positron Emission Tomography *Ph.D. thesis, University of Neuchâtel*
[97] Wyrsch N, Powolny F, Despeisse M, Dunand D, Jarron P, Ballif C 2010 Micro-Channel Plate Detectors Based on Hydrogenated Amorphous Silicon *Mater. Res. Soc. Proc. Symp.* 1245 193
[98] Beetz C P *et al.* 2000 Silicon-micromachined microchannel plates *Nucl. Instr. and Meth. In Phys. Res. A* 442 443-451
[99] Duanmu Q et al. 2001 Preparation and Performance of Si Microchannel Plate *Proc. of SPIE* 4601 284-287
[100] Marty F *et al.* 2005 Advanced etching of silicon based on deep reactive ion etching for silicon high aspect ratio microstructures and three-dimensional micro-and nanostructures *Microelectr J.* 36 673–677
[101] Franco A, Geissbühler J, Wyrsch N, Ballif C 2014 Fabrication and characterization of monolithically integrated microchannel plates based on amorphous silicon *Scientific Reports* 4 4597
[102] Franco A 2014 Monolithic Particle Detectors based on Hydrogenated Amorphous Silicon *EPFL PhD thesis* 6290

[103] Eberhardt E H 1981 An operational model for microchannel plate devices *IEEE Trans. Nucl. Sci.* 28 712–717
[104] Yeom J Wu Y Selby J C Shannon M A 2005 Maximum achievable aspect ratio in deep reactive ion etching of silicon due to aspect ratio dependent transport and the microloading effect *J. Vac. Sci. Technol.* B23 2319
[105] Mane A U *et al.* 2012 An atomic layer deposition method to fabricate economical and robust large area microchannel plates for photodetectors *Phys. Procedia* 37 722–732
[106] Lapington J S *et al.* 2009 Investigation of the secondary emission characteristics of CVD diamond films for electron amplification *Nucl. Instr. & Meth. in Phys. Res.*A610 253 - 257
[107] Fijol J J Then A M Tasker G W 1991 Secondary electron yield of SiO_2 and Si_3N_4 thin films for continuous dynode electron multipliers *Appl. Surf. Sci.* 48–49 464–471